# Deformation of hypernuclei studied with antisymmetirzed molecular dynamics

M. Isaka

*Department of Cosmosciences, Graduate School of Science,*

*Hokkaido University, Sapporo 001-0021, Japan*

M. Kimura

*Creative Research Institution (CRIS),*

*Hokkaido University, Sapporo 060-0810, Japan*

A. Dote

*Institute of Particle and Nuclear Studies,*

*KEK, Tsukuba, Ibaraki 305-0801, Japan*

A. Ohnishi

*Yukawa Institute for Theoretical Physics,*

*Kyoto University, Kyoto 606-8502, Japan*

(Dated: April 21, 2011)



## Abstract

An extended version of the antisymmetrized molecular dynamics to study structure of *p*-*sd* shell hypernuclei is developed. By using an effective $\Lambda N$ interaction, we investigate energy curves of ${}^{9}_{\Lambda}$Be, ${}^{13}_{\Lambda}$C and ${}^{20,21}_{\Lambda}$Ne as function of nuclear quadrupole deformation. Change of nuclear deformation caused by $\Lambda$ particle is discussed. It is found that the $\Lambda$ in *p*-wave enhances nuclear deformation, while that in *s*-wave reduces it. This effect is most prominent in ${}^{13}_{\Lambda}$C. The possibility of the parity inversion in ${}^{20}_{\Lambda}$Ne is also examined.

PACS numbers: Valid PACS appear here

## I. INTRODUCTION

One of the unique and interesting aspects of hypernuclei is the structure change caused by the hyperon as an impurity. Many theoretical works have suggested such phenomena caused by $\Lambda$ particle as the change of deformation [1–5], the shrinkage of the inter-cluster distance [1, 2] and the super-symmetric (genuine) hypernuclear state [2, 6–9]. Owing to the experimental developments some of them have been observed in light $p$-shell hypernuclei. As examples, we can refer to the reduction of B($E2$) in ${}^{7}_{\Lambda}$Li [10] and the identification of the super-symmetric (genuine) hypernuclear state in ${}^{9}_{\Lambda}$Be [11–13].

Today, we can expect that a new experimental facility of Japan Proton Accelerator Research Complex (J-PARC) will reveal the spectral information of $p$-$sd$ shell and neutron-rich hypernuclei. Since these normal nuclei have a variety of structure such as coexistence of shell and cluster structure [14–16] and novel exotic clustering [17–21], there must be many interesting phenomena peculiar to hypernuclei to be found. Indeed, several pioneering works predicted exotic structure in $sd$-shell hypernuclei such as the parity inversion in ${}^{20}_{\Lambda}$Ne [7] and various rotational bands in ${}^{21}_{\Lambda}$Ne [22]. These works are based on rather limited knowledge on the $\Lambda$N interaction. Since our knowledge of $\Lambda$N interaction has been greatly increased by the recent theoretical and experimental efforts [13, 23–27], we are now able to perform more quantitative and systematic study of the structure change in $\Lambda$ hypernuclei. It will reveal the dynamics and many interesting aspects of baryon many-body problem.

To perform systematic and quantitative study of $sd$-shell and neutron-rich $\Lambda$ hypernuclei, we develop an extended version of the antisymmetrized molecular dynamics (AMD) [18, 28–31], which we shall call HyperAMD. AMD has been successful to describe various exotic structure of neutron-rich nuclei and highly excited states of stable nuclei. Therefore, HyperAMD is suitable to describe the structure change and exotic structure of hypernuclei.

In this study, we introduce HyperAMD and focus on the change of nuclear quadrupole deformation caused by a $\Lambda$ particle. By applying HyperAMD to ${}^{9}_{\Lambda}$Be, ${}^{13}_{\Lambda}$C, ${}^{20}_{\Lambda}$Ne and ${}^{21}_{\Lambda}$Ne with YNG-ND $\Lambda$N interaction [32], it is found that $\Lambda$ particle changes nuclear quadrupole deformation. While the $\Lambda$ particle in $s$-wave reduces quadrupole deformation as expected, that in $p$-orbital increases it. Among the calculated hypernuclei, ${}^{13}_{\Lambda}$C has shown the most drastic change of the nuclear deformation. It is also found that the binding energy of $\Lambda$ particle depends on the structure of the core nucleus. Namely, the $\Lambda$ in $s$-wave coupled

to the deformed core nucleus has smaller binding than that coupled to spherical core. On the contrary, the $\Lambda$ in $p$-wave coupled to the deformed core has larger binding than that coupled to the spherical core. This contradicts to the preceding study [7] in which the parity inversion of ${}^{20}_{\Lambda}$Ne is predicted.

This paper is organized as follows. In the next section, we explain the theoretical framework of HyperAMD. In the section III, the change of energy curves as function of quadrupole deformation are presented. The trend of the change and its origin are discussed. The final section summarizes this work.

## II. THEORETICAL FRAMEWORK

In this section, we introduce the theoretical framework of HyperAMD. Compared to the coupled channel AMD which describes the multi-strangeness system [33], it has better description of the hyperon single particle wave function, but it does not treat multi-strangeness and is limited to single $\Lambda$ hypernuclei.

### A. Wave function

A single $\Lambda$ hypernucleus consists of $A$ nucleons and a $\Lambda$ particle is described by the wave function that is the eigenstate of the parity,

$$\Psi^{\pm} = \hat{P}^{\pm}\Psi_{\rm int}, \tag{1}$$

where $\hat{P}^{\pm}$ is the parity projector, and the intrinsic wave function $\Psi_{\rm int}$ is given by the direct product of the $\Lambda$ single particle wave function $\varphi_\Lambda$ and the wave function of $A$ nucleons $\Psi_N$,

$$\Psi_{\rm int} \ = \ \varphi_\Lambda \otimes \Psi_N. \tag{2}$$

The nuclear part is described by a Slater determinant of nucleon single particle wave packets,

$$\Psi_N \ = \ \frac{1}{\sqrt{A!}} \det\left\{\psi_i(\boldsymbol{r}_j)\right\}, \tag{3}$$

$$\psi_i(\boldsymbol{r}_j) \ = \ \phi_i(\boldsymbol{r}_j)\cdot\chi_i\cdot\eta_i, \tag{4}$$

$$\phi_i(\boldsymbol{r}) \ = \ \prod_{\sigma=x,y,z}\left(\frac{2\nu_\sigma}{\pi}\right)^{1/4}\exp\left\{-\nu_\sigma\left(r-Z_i\right)_\sigma^2\right\}, \tag{5}$$

$$\chi_i \ = \ \alpha_i\chi_\uparrow + \beta_i\chi_\downarrow, \tag{6}$$

$$\eta_i \ = \ \text{proton or neutron}, \tag{7}$$

where $\psi_i$ is the $i$-th nucleon single-particle wave packet consists of spatial $\phi_i$, spin $\chi_i$ and isospin $\eta_i$ parts. The spatial part $\phi_i$ is represented by a deformed Gaussian. Its centroid $\boldsymbol{Z}_i$ is a complex valued three-dimensional vector. The width parameters $\nu_\sigma$ are real numbers and take independent value for each direction, but are common to all nucleons. The spin part is parameterized by the complex parameters $\alpha_i$ and $\beta_i$, and the isospin part is fixed to proton or neutron. $\boldsymbol{Z}_i$, $\nu_\sigma$, $\alpha_i$ and $\beta_i$ are the variational parameters of the nuclear part.

To describe various wave functions of the $\Lambda$ particle, the $\Lambda$ single particle wave function is represented by the superposition of Gaussian wave packets,

$$\varphi_\Lambda(\boldsymbol{r}) = \sum_{m=1}^{M} c_m \varphi_m(\boldsymbol{r}), \quad \varphi_m(\boldsymbol{r}) = \phi_m(\boldsymbol{r}) \cdot \chi_m, \tag{8}$$

$$\phi_m(\boldsymbol{r}) = \prod_{\sigma=x,y,z} \left(\frac{2\nu_\sigma \rho}{\pi}\right)^{1/4} \exp\left\{-\nu_\sigma \rho \big(r - z_m\big)_\sigma^2\right\}, \tag{9}$$

$$\chi_m = a_m \chi_\uparrow + b_m \chi_\downarrow, \tag{10}$$

$$\rho \equiv \frac{m_\Lambda}{m_N}. \tag{11}$$

Again, each wave packet is parametrized by the centroid of Gaussian $\boldsymbol{z}_m$, the spin direction $a_m$ and $b_m$. $\boldsymbol{z}_m$, $a_m$, $b_m$ and $c_m$ are the variational parameters of the $\Lambda$ part. The width parameter $\nu_\sigma$ are equal to those of nuclear part. The number of the superposition $M$ is taken to be large enough to have the energy convergence of the variational calculation.

### B. Hamiltonian

The Hamiltonian used in this study is given as

$$\hat{H} = \hat{T}_N + \hat{V}_{NN} + \hat{V}_{Coul} + \hat{T}_\Lambda + \hat{V}_{\Lambda N} - \hat{T}_g. \tag{12}$$

Here, $\hat{T}_N$, $\hat{T}_\Lambda$ and $\hat{T}_g$ are the kinetic energies of nucleons, $\Lambda$ particle and the center-of-mass motion. Since we have superposed Gaussian wave packets to describe the $\Lambda$ single particle wave function, it is rather time consuming to remove the spurious motion of the center-of-mass exactly. To reduce the spurious motion, we keep the center-of-mass of wave packets at the origin of the coordinate,

$$\sum_{i=1}^{A} \boldsymbol{Z}_i + \sum_{m=1}^{M} \sqrt{\rho} \boldsymbol{z}_m = 0. \tag{13}$$

We expect that the spurious energy is not large in *sd*-shell hypernuclei, since the number of nucleons is much larger than the hyperon. A similar method is also applied in the other AMD studies [28].

Our model wave function is designed to describe the low-momentum phenomena as in the case of the conventional shell model and we shall use the low-momentum effective interaction. We have used the Gogny D1S interaction [34] as an effective nucleon-nucleon interaction $\hat{V}_{NN}$, that has been successfully applied to the stable and unstable normal nuclei. As an effective ΛN interaction, we have used the central part of the YNG-ND interaction [32]. The YNG-ND interaction depends on the nuclear Fermi momentum $k_F$ through the density-dependence of the G-matrix in nuclear medium. In this work, we apply respectively $k_F$=1.14 and 1.17 fm$^{-1}$ for ${}^{9}_{\Lambda}$Be and ${}^{13}_{\Lambda}$C, that are so determined to approximately reproduce the binding energy of Λ in *s*-wave. For ${}^{20}_{\Lambda}$Ne and ${}^{21}_{\Lambda}$Ne, we apply the same value as ${}^{13}_{\Lambda}$C, since there is no experimental data. The Coulomb interaction is approximated by the sum of seven Gaussians.

### C. Frictional cooling method with constraints

Using the frictional cooling method, the variational parameters of the model wave function are so determined that the total energy is minimized under the constraints. We have imposed two constraints on the variational calculation. The first is on the nuclear quadrupole deformation parameter $\beta$ that is achieved by adding the parabolic potential,

$$\langle \hat{V}_\beta \rangle = v_\beta (\beta - \beta_0)^2, \tag{14}$$

to the total energy. Here $\beta$ denotes the quadrupole deformation of the nuclear wave function $\Psi_N$ [28]. The deformation of nuclear part becomes equal to $\beta_0$ after the variation. It is noted that there are no constraint on the nuclear quadrupole deformation $\gamma$ and the deformation of the Λ single particle wave function. They have the optimum value after the variational calculation for each given value of $\beta_0$.

Another constraint is on the Λ single particle wave function,

$$\hat{V}_s = \Lambda |\varphi_s\rangle\langle\varphi_s|, \tag{15}$$

$$\langle \boldsymbol{r}|\varphi_s\rangle = \exp\{-\rho\bar{\nu} r^2\}, \tag{16}$$

$$\bar{\nu} = \sqrt[3]{\nu_x \nu_y \nu_z} \tag{17}$$

By using sufficiently large value for $\Lambda$, this potential forbids the $\Lambda$ in $s$-wave. Therefore, by switching off and on this potential, we respectively obtain the hypernuclear state in which a $\Lambda$ particle dominantly occupies in $s$- and $p$-waves.

The total energy plus constraint potentials,

$$E' = \frac{\langle\Psi^{\pm}|\hat{H}|\Psi^{\pm}\rangle}{\langle\Psi^{\pm}|\Psi^{\pm}\rangle} + \langle\hat{V}_s\rangle + \langle\hat{V}_\beta\rangle \tag{18}$$

is minimized using the frictional cooling method. The imaginary time development equations of the variational parameters are given as,

$$\frac{dX}{dt} = \frac{\mu}{\hbar}\frac{\partial E'}{\partial X^*}, \tag{19}$$

$$X = \boldsymbol{Z}_i, \boldsymbol{z}_m, \alpha_i, \beta_i, a_m, b_m, \nu_\sigma, \nu_i^\Lambda, \tag{20}$$

where $\mu$ is arbitrary negative real number. It is easy to proof that $E'$ decreases as time develops, and after sufficient time steps we obtain the energy minimum under the constraint. By this method, we obtain the hypernuclear wave function for given $\beta_0$, the total parity and the $\Lambda$ single particle orbital. In the present work, $\Lambda$ dominantly occupies $s$- or $p$-wave and we shall use the notation $\Lambda_s$ and $\Lambda_p$ for them. Combined with the parity projection, we obtain four different configurations in which $\Lambda_s$ and $\Lambda_p$ couple to the positive- and negative-parity states of the core. They are denoted as $\Psi_N^+ \otimes \Lambda_s$, $\Psi_N^- \otimes \Lambda_s$, $\Psi_N^+ \otimes \Lambda_p$ and $\Psi_N^- \otimes \Lambda_p$ in the following.

## III. RESULTS AND DISCUSSIONS

### A. general trend of the energy curves

We have performed the variational calculation for ${}^{9}_{\Lambda}$Be, ${}^{13}_{\Lambda}$C, ${}^{20}_{\Lambda}$Ne and ${}^{21}_{\Lambda}$Ne. To illustrate the change of nuclear deformation, Figure 1 shows energy curves of hypernuclear states with different configurations and corresponding normal nuclei as functions of deformation $\beta$. Each energy curve has an energy minimum shown by the open circle, and the binding energies, quadrupole deformation and radius at the minimum are listed in Table I. The binding energy of $\Lambda$ is defined as the difference of energy between the ground state of the core nucleus and the hypernuclear states,

$$B_\Lambda = B({}^{A+1}_{\Lambda}X) - B({}^{A}X_{g.s.}) \tag{21}$$

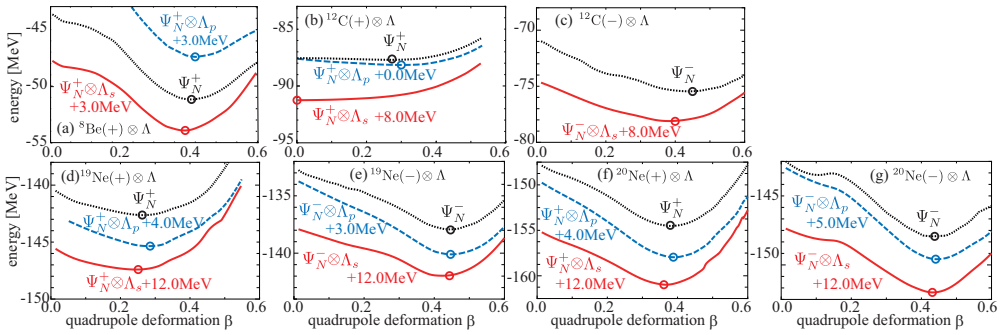


FIG. 1: (color online) Energy curves as function of nuclear quadrupole deformation $\beta$ for (a) ${}^{9}_{\Lambda}$Be, (b)(c) ${}^{13}_{\Lambda}$C, (d)(e) ${}^{20}_{\Lambda}$Ne and (f)(g) ${}^{21}_{\Lambda}$Ne. (a),(b),(d) and (f) compare the positive-parity states of normal nuclei ($\Psi_N^+$) with the hypernuclear states of $\Psi_N^+ \otimes \Lambda_s$ and $\Psi_N^+ \otimes \Lambda_p$ configurations. (c),(e) and (f) compare the negative-parity states ($\Psi_N^-$) with the hypernuclear states of $\Psi_N^- \otimes \Lambda_s$ and $\Psi_N^- \otimes \Lambda_p$ configurations. Open circle shows the energy minimum on each curve. Energies of hypernuclei are shifted as shown in the figure for the sake of the presentation.

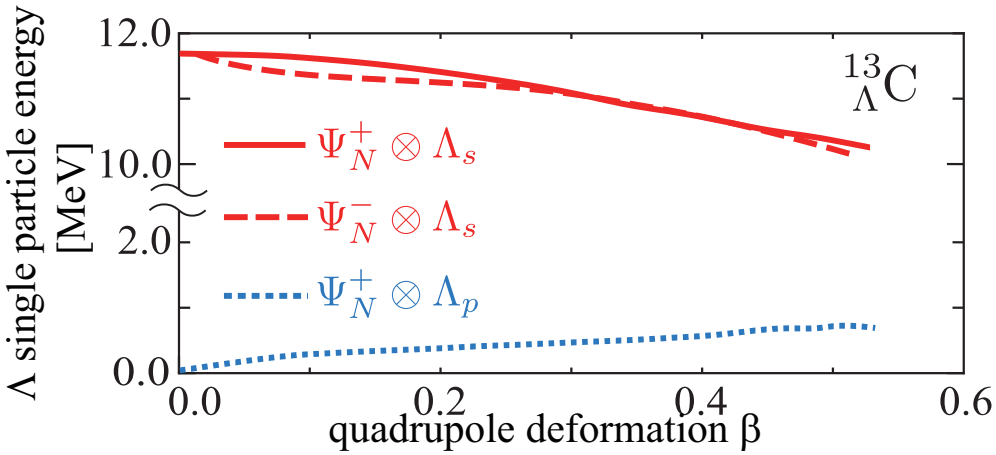


FIG. 2: (color online) The single particle energy of $\Lambda_s$ and $\Lambda_p$ of ${}^{13}_{\Lambda}$C as function of the quadrupole deformation of core nucleus $^{12}$C. Solid (dashed) line shows the energy of $\Lambda_s$ coupled to the positive (negative) parity state of $^{12}$C. Dotted line shows the energy of $\Lambda_p$ coupled to the negative-parity state of $^{12}$C.

As the general trend, the shape of energy curve is not strongly modified by $\Lambda$ particle except for ${}^{13}_{\Lambda}$C, and deformation $\beta$ at the minima are slightly changed. In all cases, $\Lambda_s$ reduces quadrupole deformation. This is consistent with the cluster model calculations [22, 27] and the (relativistic) mean-field calculations [3–5] that demonstrated the reduction of $\beta$ by

TABLE I: Calculated total and $\Lambda$ binding energies $B$, $B_\Lambda$ in MeV, quadrupole deformation parameters $\beta$ and $\gamma$, and the root mean square radius in fm at the minimum of each energy curve. Central values of observed energies [12, 13, 35, 36] are also listed in parenthesis. The energies for $\Lambda_p$ states of ${}^{9}_{\Lambda}$Be and ${}^{13}_{\Lambda}$C are estimated from the observed excitation energies given in Ref. [13].

| | | $B$ | $B_\Lambda$ | $\beta$ | $\gamma$ | $\sqrt{\langle r^2 \rangle}$ |
|---|---|---|---|---|---|---|
| ${}^{8}$Be | $\Psi^+_N$ | 51.2 (56.5) | - | 0.68 | 1.9 | 2.50 |
| ${}^{9}_{\Lambda}$Be | $\Psi^+_N \otimes \Lambda_s$ | 56.9 (63.2) | 5.75 (6.71) | 0.65 | 1.9 | 2.44 |
| | $\Psi^+_N \otimes \Lambda_p$ | 50.4 (56.7) | -0.77 (0.19) | 0.71 | 1.7 | 2.53 |
| ${}^{12}$C | $\Psi^+_N$ | 87.7 (92.2) | - | 0.27 | 60.0 | 2.42 |
| | $\Psi^-_N$ | 75.5(82.5) | - | 0.45 | 45.4 | 2.56 |
| ${}^{13}_{\Lambda}$C | $\Psi^+_N \otimes \Lambda_s$ | 99.3 (103.9) | 11.6 (11.69) | 0.00 | - | 2.32 |
| | $\Psi^+_N \otimes \Lambda_p$ | 88.2 (93.8) | 0.46 (1.65) | 0.30 | 55.1 | 2.42 |
| | $\Psi^-_N \otimes \Lambda_s$ | 86.2 | -1.5 | 0.40 | 42.5 | 2.49 |
| ${}^{19}$Ne | $\Psi^+_N$ | 142.6(143.7) | - | 0.27 | 0.6 | 2.81 |
| | $\Psi^-_N$ | 137.9(143.5) | - | 0.45 | 0.5 | 2.91 |
| ${}^{20}_{\Lambda}$Ne | $\Psi^+_N \otimes \Lambda_s$ | 159.4 | 16.8 | 0.25 | 0.6 | 2.76 |
| | $\Psi^+_N \otimes \Lambda_p$ | 148.4 | 5.74 | 0.30 | 0.9 | 2.81 |
| | $\Psi^-_N \otimes \Lambda_s$ | 154.0 | 11.4 | 0.45 | 0.5 | 2.87 |
| | $\Psi^-_N \otimes \Lambda_p$ | 144.2 | 1.6 | 0.45 | 0.5 | 2.89 |
| ${}^{20}$Ne | $\Psi^+_N$ | 155.6(160.6) | - | 0.38 | 0.7 | 2.89 |
| | $\Psi^-_N$ | 147.5(155.6) | - | 0.43 | 0.4 | 2.91 |
| ${}^{21}_{\Lambda}$Ne | $\Psi^+_N \otimes \Lambda_s$ | 172.8 | 17.2 | 0.37 | 0.7 | 2.85 |
| | $\Psi^+_N \otimes \Lambda_p$ | 162.4 | 6.75 | 0.38 | 0.6 | 2.88 |
| | $\Psi^-_N \otimes \Lambda_s$ | 164.5 | 8.9 | 0.42 | 0.4 | 2.88 |
| | $\Psi^-_N \otimes \Lambda_p$ | 154.6 | 7.1 | 0.43 | 0.4 | 2.90 |

$\Lambda_s$. On the other hand, it is found that $\Lambda_p$ increases $\beta$. The magnitude of the change in quadrupole deformation is strongly dependent on the core nucleus, and the most prominent in ${}^{13}_{\Lambda}$C in which $\Lambda_s$ makes ${}^{12}$C core spherical, while $\Lambda_p$ enhances the core deformation. The reason of the opposite behavior of $\Lambda_s$ and $\Lambda_p$ and the strong dependence on the core nucleus

is clearly seen in the single particle energy of Λ. Figure 2 shows the single particle energy of Λ ($\epsilon_\Lambda(\beta)$) in each parity and Λ single particle state in ${}^{13}_{\Lambda}$C. Here $\epsilon_\Lambda(\beta)$ is defined as the difference between the binding energy of ${}^{13}_{\Lambda}$C with the deformation $\beta$ and that of corresponding state of ${}^{12}$C with the same deformation,

$$\epsilon_\Lambda(\beta) = B_{{}^{13}_{\Lambda}\mathrm{C}}(\beta) - B_{{}^{12}\mathrm{C}}(\beta). \tag{22}$$

It shows the Nilsson-model-like behavior of the Λ single particle energy. The binding of $\Lambda_s$ becomes shallower as deformation becomes larger. In the case of $\Lambda_p$, Λ occupies the lowest $p$-wave that comes down as deformation becomes larger. Therefore, $\Lambda_s$ makes quadrupole deformation smaller and $\Lambda_p$ in the lowest $p$-wave makes it larger. The Λ single particle energy varies within a range of 1∼2 MeV as function of quadrupole deformation that is smaller than the variation of the core nucleus energy. It is also case for other calculated hypernuclei. This explains why only ${}^{13}_{\Lambda}$C (FIG. 1 (b)) manifests the drastic change in quadrupole deformation. Since the positive-parity state of ${}^{12}$C is quite soft against the quadrupole deformation, small change in the Λ single particle energy can result in the large modification in quadrupole deformation. In other cases, change in Λ single particle energy cannot overcome much larger variation of the core energy and results in minor modification of quadrupole deformation. Therefore, we can conclude that the drastic change of quadrupole deformation by Λ particle occurs when the core nucleus is quite soft against quadrupole deformation within a range of 1∼2 MeV. Since the behavior of the energy curve is sensitive to the effective NN interaction [37], the drastic change in ${}^{13}_{\Lambda}$C may depend on the choice of NN interaction and it will be investigated in our future work. The behavior of the Λ single particle energy is also understood from the density distribution of the Λ particle and the core nucleus as shown in Figure 3. It shows that as nuclear deformation becomes larger the overlap between the $\Lambda_s$ and the core wave function becomes smaller (for example, compare $\Psi^+_N \otimes \Lambda_s$ and $\Psi^-_N \otimes \Lambda_s$ of ${}^{20}_{\Lambda}$Ne). It leads to the reduction of ΛN attraction. On the contrary, larger deformation makes the overlap larger in the case of $\Lambda_p$ and increases ΛN attraction (see $\Psi^+_N \otimes \Lambda_p$ and $\Psi^-_N \otimes \Lambda_p$ of ${}^{20}_{\Lambda}$Ne). In the case of $\Lambda_p$, larger deformation reduces the kinetic energy that also contribute to the deeper binding of $\Lambda_p$.

Another issue to be mentioned is the reduction of the nuclear radius by Λ particle. In all cases, the radius of nuclear part is reduced, but the reduction (less than 5%) is much smaller than in the case of ${}^{7}_{\Lambda}$Li (20%) [10]. More detailed discusstion will be made in our

next work.

### B. discussion on each hypernucleus

The calculated total binding energies of $^{8}$Be and $^{9}_{\Lambda}$Be underestimate the observed values by about 5MeV. The underestimation is common to all other hypernuclei. It will be resolved by performing the angular momentum projection and the generator coordinate method (GCM) that are usually performed in the study of normal nuclei by AMD. Indeed, in the case of $^{20}$Ne, it was shown that AMD calculation [15] reproduces the observed binding energy. The angular momentum projection and GCM will be performed in our next work. Despite of the underestimatin of the total binding energy, $B_\Lambda$ of $\Lambda_p$ is comparable with the observed value.

The density distribution of $\Lambda_p$ in $^{9}_{\Lambda}$Be ($\Psi^{+}_{N} \otimes \Lambda_p$ in FIG. 3) clearly shows that this state corresponds to the supersymmetric (genuine) hypernuclear state [11–13]. The nuclear part has the pronouced $2\alpha$ cluster structure and the $\Lambda$ occupies the $p$ orbital parallel to the symmetry axis. It is also interesting to note that $\Lambda_s$ state reduces the inter-cluster distance, while $\Lambda_p$ state increases it.

$^{13}_{\Lambda}$C manifests the drastic change in the quadrupole deformation. The $\Lambda_s$ makes $^{12}$C core spherical, while $\Lambda_p$ state enhances deformation. It is noted that $^{12}$C has the $0p_{3/2}$ subshell closure configuration at small deformation and $3\alpha$ cluster structure develops as deformation becomes larger. In other words, the nucleon spin is not satureted at small deformation, while that is alomost zero at larger deformation. The sophisticated AMD calculation [14] has shown that the low-lying states of $^{12}$C have mixed nature between the $0p_{3/2}$ subshell closure configuration and $3\alpha$ cluster structure, and the mixing strength is different for each state. Since $\Lambda$ particle changes the deformation and spin property of $^{12}$C, it will have influence on the $\Lambda$N spin-orbit splitting of $^{13}_{\Lambda}$C [38–40].

Based on the cluster model calculation, the parity inversion in $^{20}_{\Lambda}$Ne was suggested by Sakuda and Bando [7]. The core nucleus $^{19}$Ne has the $\alpha$+$^{15}$O cluster state ($J^\pi$=$1/2^-_1$) 238 keV above the ground state ($J^\pi$=$1/2^+$) that has $(sd)^3$ shell structure [41]. They concluded that $\Lambda_s$ coupled to the $J^\pi$=$1/2^-_1$ state was more deeply bound than that coupled to the gound state, and the $J^\pi$=$1/2^- \otimes \Lambda_s$ configuration becomes the ground state of $^{20}_{\Lambda}$Ne. They argued that the $J^\pi$=$1/2^-_1$ state has dilute $\alpha$+$^{15}$O cluster structure and by the reduction of the

inter-cluster distance, $\Lambda_s$ gains larger binding energy than the $J^\pi{=}1/2_1^+ \otimes \Lambda_s$ configuration. Our result shows the opposite trend to their result. Since the positive-parity state is more deformed than the negative-parity state, the binding of $\Lambda_s$ is weaker when it coupled to the negative-parity state. This trend is common to other calculations including the cluster model calculation for ${}^{21}_{\Lambda}$Ne [22]. However, AMD fails to reproduce small excitation energy of the negative-parity state and it does not have prominent $\alpha{+}^{15}$O clustering, that are mainly due to the lack of the angular momentum projection and the GCM calculation. We will need more sophisticated AMD calculation to settle down this problem.

The negative-parity state of $^{20}$Ne has larger deformation than the positive-parity state. Therefore, the $\Lambda_s$ coupled to the positive-parity state is more deeply bound than that coupled to the negative-parity state. It is common to other hypernuclei studied here. On the contrary, $\Lambda_p$ is more deeply bound to the negative-parity state. Since number of nucleons in $^{20}$Ne is large enough to bound $\Lambda_p$, we can expect that the addition of $\Lambda$ will generate a variety of bound rotational bands in ${}^{21}_{\Lambda}$Ne as disscussed by Yamada *et al.*[22]. We will discuss ${}^{21}_{\Lambda}$Ne in detail in the forthcoming paper.

## IV. SUMMARY

An extended version of AMD named HyperAMD has been introduced to investigate structure of *p*-*sd* shell hypernuclei. The energy curves of ${}^{9}_{\Lambda}$Be, ${}^{13}_{\Lambda}$C, ${}^{20}_{\Lambda}$Ne and ${}^{21}_{\Lambda}$Ne as functions of quadrupole deformation are studied. It has been found that $\Lambda_s$ reduces nuclear deformation, while $\Lambda_p$ increases it. It is due to the variation of the single particle energy of $\Lambda$ as function of quadrupole deformation. The binding of $\Lambda_s$ decreases as deformation becomes larger, while that of $\Lambda_p$ increases. The variation of $\Lambda$ single particle energy is within a range of 1$\sim$2 MeV, that is rather small compared to the variation of the energy of the core nucleus. Therefore, the magnitude of the change of deformation strongly depends on the softness of the core nucleus against quadrupole deformation. Since $^{12}$C is very soft against quadrupole deformation, it manfests the most prominent change of quadrupole deformation. This trend of the deformation change caused by $\Lambda_s$ and $\Lambda_p$ contradicts to the cluster model calculation for ${}^{20}_{\Lambda}$Ne [7], but is consistent with other calculations. More sphisticated AMD calculation

will be needed to resolve this disagreement.

---


[1] T. Motoba, H. Bandō and K. Ikeda, Prog. Theor. Phys. **70**, 189 (1983); **71**, 222 (1984).

[2] T. Motoba, H. Bandō, K. Ikeda, and T. Yamada, Prog. Theor. Phys. Suppl. **81**, Chap. 3 (1985).

[3] Xian-Rong Zhou, H.-J. Schulze, H. Sagawa, Chen-Xu Wu and En-Guang Zhao, Phys. Rev. C**76**, 034312 (2007).

[4] M.T. Win and K. Hagino, Phys. Rev. C**78**, 054311 (2008).

[5] H.-J. Schulze, M.T. Win, K. Hagino and S. Sagawa, Prog. Theor. Phys. **123**, 569 (2010).

[6] R.H. Dalitz and A. Gal, Phys. Rev. Lett. **36**, 362 (1976).

[7] T. Sakuda and H. Bandō, Prog. Theor. Phys. **78** 1317 (1987).

[8] U. Straub, Z.Y. Zhang, K. B̈auer, A. Faessler and S.B. Khadkikar, Phys. Lett. B**200**, 241 (1988).

[9] T. Yamada, K. Ikeda, H. Bandō and T. Motoba, Phys. Rev. C**38**, 854 (1988).

[10] K. Tanida *et al.*, Phys. Rev. Lett. **86**, 1982 (2001).

[11] P. H. Pile *et al.*, Phys. Rev. Lett. **66**, 2585 (1991).

[12] O. Hashimoto *et al.*, Nucl. Phys. A**639**, 93c (1998).

[13] O. Hashimoto and H. Tamura, Prog. Part. Nucl. Phys. **57**, 564 (2006), and references therein.

[14] Y. Kanada-En'yo, Phys. Rev. Lett. **81**, 5291 (1998).

[15] M. Kimura, Phys. Rev. C**69**, 044319 (2004).

[16] M. Kimura and H. Horiuchi, Nucl. Phys. A**767**, 58 (2006).

[17] W. von Oertzen, Z. Phys. A**354**, 37 (1996).

[18] Y. Kanada-En'yo, H. Horiuchi and A. Ono, Phys. Rev. C**52**, 628 (1995).

[19] N. Itagaki and S. Okabe, Phys. Rev. C**61**, 044306 (2000).

[20] P. Descouvemomnt, Nucl. Phys. A**699**, 463 (2002).

[21] Y. Kanada-En'yo, Phys. Rev. C**66**, 011303 (2002).

[22] T. Yamada, K. Ikeda, H. Bandō and T. Motoba, Prog. Theor. Phys. **71**, 985 (1984).

[23] A. Reuver, K. Holinde and J. Speth, Nucl. Phys. A**570**, 543 (1994).

[24] T.H. Rijken and Y. Yamamoto, Phys. Rev. C**73**, 044008 (2006).

[25] Y. Fujiwara, Y. Suzuki and C. Nakamoto, Prog. Part. Nucl. Phys. **58**, 439 (2007).

[26] D.J. Millener, Nucl. Phys. A**804**, 84 (2008).

[27] E. Hiyama and T. Yamada, Prog. Part. Nucl. Phys. **63**, 339 (2009), and references therein.

[28] A. Dote, H. Horiuchi and Y. Kanada-En'yo, Phys. Rev. C**56**, 1844 (1997).

[29] Y. Sugawa, M. Kimura and H. Horiuchi, Prog. Theor. Phys. **106**, 1129 (2001).

[30] M. Kimura, Y. Sugawa and H. Horiuchi, Prog. Theor. Phys. **106**, 1153 (2001).

[31] Y. Kanada-En'yo, M. Kimura and H. Horiuchi, C.R. Physique **4**, 497 (2003).

[32] Y. Yamamoto, T. Motoba, H. Himeno, K. Ikeda and S. Nagata, Prog. Theor. Phys. Suppl. **117**, 361 (1994).

[33] H. Matsumiya, M. Kimura, A. Dote and H. Ohnishi, submitted to Phys. Rev. C.

[34] J. Dechagé and D. Gogny, Phys. Rev. C**21**, 1568 (1980).

[35] M. Juric *et al.*, Nucl. Phys. B**52**, 1 (1973).

[36] D. H. Davis, Nucl. Phys. A **547**, 369c (1992).

[37] J. A. Maruhn *et al.*, Phys. Rev. C**74**, 044311 (2006).

[38] S. Ajimura, *et al.*, Phys. Rev. Lett. **86**, 4255 (2001).

[39] E. Hiyama, M. Kamimura, T. Motoba, T. Yamada and Y. Yamamoto, Phys. Rev. Lett. **85**, 270 (2000).

[40] D.J. Millener, Nucl. Phys. A **691**, 93c (2001).

[41] T. Sakuda and F. Nemoto, Prog. Theor. Phys. **62**, 1274 (1979); **62**, 1606 (1979).

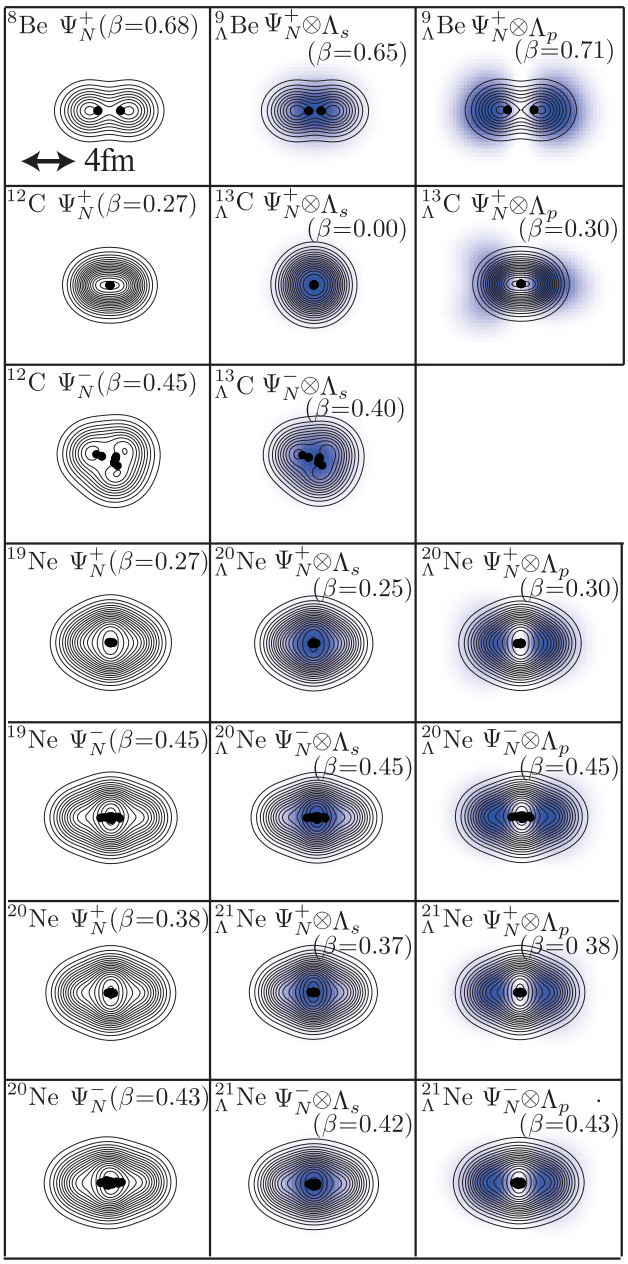


FIG. 3: (color online) Density plot of the intrinsic wave function at each minimum on the energy curve. Contour lines shows the density of the nuclear part $\Psi_N$ and the color plot shows the $\Lambda$ single particle orbital $\varphi_\Lambda$. Dots in the figure shows the centroids of Gaussian wave packets on nuclear part $\Psi_N$.